Appendix B: Sensor Optimization

B.0 Global Optimization with Massless Support

In this appendix, we calculate the shape of the detector magnet that optimizes sensitivity in a measurement of a spherical sample's average magnetization given a condition of closest approach to the sample's surface. The quantity to be optimized is the signal-to-noise ratio of the measurement, which we defined in Chapter 2 (Equation (2.6)):

$$SNR_{\mathrm{BOOM}} = F_{\mathrm{z,rms}}/F_{\mathrm{N}} \; . \tag{B.1}$$

We begin by parameterizing the shape of the detector. Symmetry requires that the detector be a solid of revolution about the axis along which it will be displaced, which we take to be the *z*-axis. Figure B.1 shows a detector magnet above a spherical sample, with a distance of closest approach, R_{max}, defined along the *z*-axis relative to the center of the sample. We also take the center of the sample to be

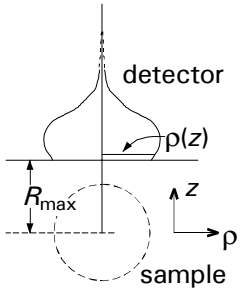

Figure B.1. Curve defining the detector magnet, which is a solid of revolution.

the origin of a cylindrical coordinate system. The most general parameterization of the sensor magnet's shape given the symmetry restriction is a function,

$$\rho = \rho(z), \tag{B.2}$$

that defines the surface of the sensor magnet. This function is single-valued, greater than or equal to zero everywhere, and defined on the interval $\{z \mid R_{\max} \le z < \infty\}$, but is otherwise unrestricted.

The total root-mean-squared (rms) force on the detector is the integral of the forces on dipole elements in the detector,

$$F_{z,\mathrm{rms}} = \frac{w}{\sqrt{2}} \int_{\substack{\text{detector} \\ \text{volume}}} \hat{\mathbf{z}} \cdot \mathbf{dF}, \tag{B.3}$$

reduced by the factor $\sqrt{2}$ relative to the static force and scaled by a factor w, which accounts for the amplitude of the Fourier component of the force for a specfic driving protocol (see Chapter 2). Due to the cylindrical symmetry of the system, only the z-components of the forces add in concert, and so, following Chapter 2, we sum up the contributions of the z components only. The integrand in Equation (B.3) may be written (see Chapter 2)

$$\hat{\mathbf{z}} \cdot \mathbf{dF} = \frac{\mu_0}{4\pi} \frac{V_s M_s M_d}{r^4} \left(9 - 15\cos^2\theta\right)\cos\theta dV_d, \tag{B.4}$$

where V_s is the sample's volume, M_s is its magnetization, M_d is the magnetization of the detector magnet, $r = \sqrt{z^2 + \rho^2}$ is the distance of the given detector dipole from

the origin, and θ is the polar angle at the location of the detector dipole. With the substitutions $r^2 = z^2 + \rho^2$, $\cos\theta = \frac{z}{r}$, and $dV_d = \rho d\rho d\phi dz$, we may write

$$F_{z,rms} = \frac{w}{\sqrt{2}} \frac{\mu_0}{4\pi} V_s M_s M_d \int_0^{2\pi} d\phi \int_{R_{max}}^{\infty} z dz \int_0^{\rho(z)} \frac{9\rho^2 - 6z^2}{\left(z^2 + \rho^2\right)^{7/2}} \rho d\rho \tag{B.5}$$

for the rms force. Evaluating the integrals over ρ and the azimuthal angle φ, we find

$$F_{z,rms} = -\frac{3}{2} \frac{w}{\sqrt{2}} \mu_0 M_s M_d V_s \int_{R_{max}}^{\infty} f(z, \rho(z)) dz \,, \tag{B.6}$$

where

$$f(z, \rho(z)) = \frac{z\rho^2}{r^5} \tag{B.7}$$

and

$$r = r(z) = \sqrt{z^2 + \rho(z)^2} \,. \tag{B.8}$$

Equation (B.6) shows that the signal force $F_{z,rms}$ is a functional whose value depends on the parameterizing relation $\rho = \rho(z)$. The noise force F_N in the denominator of Equation (B.1) is also a functional of ρ. To find this functional, we first write

$$F_N = \sqrt{4 k_B T \alpha \Delta f} \,, \tag{B.9}$$

where T is the temperature of the detector oscillator, Δf is the bandwidth of the measurement, and α is the oscillator's damping constant (Equation (2.8)). α is proportional to the oscillator's motional mass m, which we assume is dominated by the mass of the magnetic detector. (In section B.1 we relax this assumption for the simpler case of a right circular cylinder.) For a magnet with cylindrical symmetry, α

can be written in terms of the damping rate γ, the density η of the detector material, and the volume of the magnet:

$$\alpha = m\gamma = \gamma\eta \int_{\substack{\text{detector}\\ \text{volume}}} dV = \gamma\eta \int_{R_{\max}}^{\infty} \pi\rho^2 dz = \pi\gamma\eta \int_{R_{\max}}^{\infty} v(z,\rho(z))dz \,. \tag{B.10}$$

where
$$v(z,\rho(z)) = \rho^2 \,. \tag{B.11}$$

The explicit definition of the symbols *f* and *v* for the integrands in Equations (B.7) and (B.11) will help simplify the notation in the discussion that follows.

Now, let

$$\tilde{J} = SNR_{\text{BOOM}}^2 = \frac{F_{\text{z,rms}}^2}{F_{\text{N}}^2} \,. \tag{B.12}$$

Substituting in the expressions for the signal and noise forces and collecting constant factors that do not depend on the shape function ρ, we write

$$\tilde{J} = \left(\frac{9}{32\pi} \frac{w^2 \mu_0^2 M_{\text{s}}^2 M_{\text{d}}^2 V_{\text{s}}^2}{k_{\text{B}} T \eta \gamma \Delta f} \right) J \tag{B.12}$$

and
$$J = \frac{F^2}{V} \,, \tag{B.13}$$

where
$$F = \int_{R_{\max}}^{\infty} f(z,\rho(z))dz \quad \text{and} \quad V = \int_{R_{\max}}^{\infty} v(z,\rho(z))dz \,. \tag{B.14a,b}$$

The optimal sensor shape is defined by the function $\rho(z)$ that extremizes the signal-to-noise ratio. Since all we have done is to square SNR_{BOOM} and remove constant factors in deriving Equation (B.13), a necessary and sufficient condition is

that J is extremized. To find the optimum function $\rho(z)$, we consider the variation δJ in J caused by arbitrary infinitesimal variations in $\rho(z)$ about its optimum. When $\rho(z)$ is optimal, J is stationary with respect to these variations, and so in accordance with Equation (B.13) we write

$$\delta J = \frac{2VF\delta F - F^2\delta V}{V^2} = \frac{F}{V^2}\left(2V\delta F - F\delta V\right) = 0\,. \tag{B.15}$$

Since neither of the integrals F nor V are zero, we must have

$$2V\delta F - F\delta V = 0\,, \tag{B.16}$$

where, since the limits on the integrals are fixed,

$$\delta F = \int_{R_{\max}}^{\infty} \delta f(z,\rho)dz \quad \text{and} \quad \delta V = \int_{R_{\max}}^{\infty} \delta v(z,\rho)dz\,. \tag{B.17a,b}$$

The variations in the integrands are directly proportional to the functional variation $\delta\rho$ in $\rho = \rho(z)$:

$$\delta f = \frac{\partial f}{\partial \rho}\delta\rho\,;\ \delta v = \frac{\partial v}{\partial \rho}\delta\rho\,, \tag{B.18a,b}$$

where

$$\frac{\partial f}{\partial \rho} = \frac{z\rho}{\left(z^2+\rho^2\right)^{7/2}}\left(2z^2 - 3\rho^2\right) \tag{B.19}$$

and

$$\frac{\partial v}{\partial \rho} = 2\rho\,. \tag{B.20}$$

Using Equations (B.17–18), we may rewrite Equation (B.16) as

$$2V\int_{R_{\max}}^{\infty}\frac{\partial f}{\partial \rho}\delta\rho dz - F\int_{R_{\max}}^{\infty}\frac{\partial v}{\partial \rho}\delta\rho dz = 0 \tag{B.21}$$

or, since V and F are just numbers (functionals of $\rho(z)$),

$$\int_{R_{\max}}^{\infty} \left(2V \frac{\partial f}{\partial \rho} - F \frac{\partial v}{\partial \rho} \right) \delta\rho \, dz = 0 \qquad \text{(B.22)}$$

According to the fundamental theorem of the calculus of variations[1], in order for this integral to vanish for *arbitrary* variations $\delta\rho$ in the shape function $\rho(z)$, we must have

$$2V \frac{\partial f}{\partial \rho} - F \frac{\partial v}{\partial \rho} = 0 \, . \qquad \text{(B.23)}$$

Equation (B.23) is analogous to the Euler-Lagrange equations that result from extremizing action in the Lagrangian formulation of mechanics. It is worth recalling that this equation is a prescription for solving for that function $\rho = \rho(z)$ which satisfies an extremum principle, in this case the optimal signal-to-noise ratio. Note that, in contrast to Euler-Lagrange equations (and other such equations as arise in the calculus of variations, like the so-called "brachistochrone" problem[2]), Equation (B.23) is not a differential equation, as the derivative $\rho'(z)$ appears nowhere in (B.23). It is in fact an integral equation that has in it the functionals $F[\rho(z)]$ and $V[\rho(z)]$, which are *numbers*, and not functions of the variable z *per se*.

With the help of equations (B.19, 20, and 8), we rewrite Equation (B.23) in the form:

$$\frac{F}{2V} = \frac{\partial f / \partial \rho}{\partial v / \partial \rho} = \frac{1}{2} \frac{z}{r^7} \left(5z^2 - 3r^2 \right). \qquad \text{(B.24)}$$

The left-hand side of Equation (B.24) is a *number*, a functional of the whole function $\rho(z)$, and not an explicit function of z, and therefore the right-hand side may be set equal to a constant:

$$\lambda^{-4} \equiv \frac{F}{2V} = \frac{1}{2}\frac{z}{r^7}\left(5z^2 - 3r^2\right). \tag{B.25}$$

An even power of λ is allowed because the right hand side is never less than zero. The quartic exponent is chosen so that λ will have the dimensions of length (λ's significance will become clear shortly).

Equation (B.25) can be viewed as a relation that defines the function $\rho(z)$ implicitly, but it is best solved as an equation for $r = r(z(\theta)) = \sqrt{z(\theta)^2 + \rho(z(\theta))^2}$ in terms of $\theta = \arccos(z/r)$:

$$\left(\frac{r}{\lambda}\right)^4 = \frac{1}{2}\left(5\cos^3\theta - 3\cos\theta\right) = P_3(\cos\theta). \tag{B.26}$$

This is the shape that optimizes the signal-to-noise ratio given the condition of closest approach, and all that is left is to find the parameter λ in terms of R_{max}. When $\theta = 0$, we have $r = \lambda$, and so λ is the distance from the center of the sample (which is also the origin of the coordinate system) to the top of the sensor magnet. The optimal shape is shown in Figure B.2.

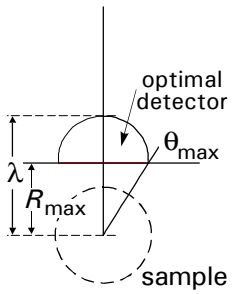

Figure B.2. Optimal shape for the detector magnet.

To find λ, we recognize that, in Equation (B.25), we have both an integral equation,

$$\lambda^{-4} = \frac{F}{2V} = \frac{\int_{R_{\max}}^{\lambda} \frac{z\rho^2}{r^5}\, dz}{2\int_{R_{\max}}^{\lambda} \rho^2 dz}, \tag{B.27}$$

and a functional form for r (and therefore z and ρ) as a function of θ (which we have already recast in the form of Equation (B.26)) that we can substitute directly into the integrands. Note also that the limits on z have been written $\{z \mid R_{\max} \le z < \lambda\}$, since the function $\rho = \rho(z)$ is zero for values of z greater than λ. We first multiply Equation (B.27) by λ times the denominator of the right-hand side, rearrange, and find

$$2\lambda^{-3}\int_{R_{\max}}^{\lambda} \rho^2 dz - \lambda\int_{R_{\max}}^{\lambda} \frac{z\rho^2}{r^5}\, dz = \int_{R_{\max}}^{\lambda} \left(2\lambda^{-2}\rho^2 - \lambda^2\,\frac{z\rho^2}{r^5}\right)\lambda^{-1} dz = 0\,. \tag{B.28}$$

The latter integral (which is dimensionless in anticipation of a later substitution) may now be rewritten with the substitutions

$$\rho = r(\theta)\sin\theta\,, \quad z = r(\theta)\cos\theta\,,$$

and

$$dz = \left(r'(\theta)\cos\theta - r(\theta)\sin\theta\right)d\theta\,. \tag{B.29a,b,c}$$

The result is

$$\int_{\theta_{\max}}^{0} \left(\frac{2r^2\,\sin^2\theta}{\lambda^2} - \frac{\lambda^2\cos\theta\sin^2\theta}{r^2}\right)\frac{r}{\lambda}\left(\frac{r'(\theta)}{r}\cos\theta - \sin\theta\right)d\theta = 0\,. \tag{B.30}$$

The limits R_{max} and λ have been replaced by the corresponding θ values θ_{max} and 0 (see Figure B.2). In combination with Equation (B.26), which expresses r/λ as a function of θ, Equation (B.30) is an integral equation for the angle θ_{max}. To solve it, we implicitly differentiate Equation (B.26) and find that

$$\frac{r'(\theta)}{r} = \frac{3}{4}\frac{1-5\cos^2\theta}{5\cos^3\theta - 3\cos\theta}\sin\theta\,. \tag{B.31}$$

Substituting Equations (B.26) and (B.31) into (B.30), we obtain

$$\frac{5\cdot 2^{1/4}}{4}\int_0^{\theta_{max}} \frac{\left(5\cos^2\theta-4\right)\left(1-\cos^2\theta\right)\left(3-7\cos^2\theta\right)\cos^2\theta}{\left(5\cos^3\theta-3\cos\theta\right)^{5/4}}\sin\theta d\theta = 0\,, \tag{B.32}$$

which can be solved numerically, yielding $\cos\theta_{max} \approx 0.84913$ (or $\theta_{max} \approx 31.88°$).

Now, $z = R_{max}$ when $\theta = \theta_{max}$, and so, substituting $r = z\sec\theta$ into Equation (B.26) we find

$$\left(\frac{R_{max}\sec\theta_{max}}{\lambda}\right)^4 = \frac{1}{2}\left(5\cos^3\theta_{max} - 3\cos\theta_{max}\right), \tag{B.33}$$

whose solution is $\lambda \approx 1.6542\,R_{max}$. Figure B.2 is drawn consistent with this ratio.

A sensor magnet shaped as in Figure B.2 is a global optimum as regards sensitivity (given that the motional mass is dominated by that of the magnetic material), but other considerations render it impractical for BOOMERANG. Large static forces would result from placing such a "mushroom-cap" magnet inside a suitable annulus, and homogeneity through the sample volume would be compromised were this shape used instead of the optimal right circular cylinder, or "hockey-puck" of Chapter 2. Fortunately, the sensitivity of the best hockey-puck

design is about 72% of the globally optimal mushroom-cap design and about 36% better than an optimized spherical sensor magnet (all constrained by the same R_{max}). The close match in size between the optimal cylinder and the global optimum is shown in Figure B.3. The near-optimal sensitivity of the hockey puck, in combination with its superior homogeneity and relative ease of manufacture at the millimeter size scale and below make it the best choice for the sensor magnet's shape.

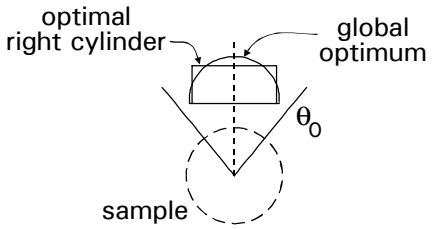

Figure B.3. Optimal shape for the detector magnet compared to optimal right cylinder. The sensitivity of the cylinder is nearly (about 72%) the optimal sensitivity. The nodal surface at polar angle θ_0 described in Chapter 2 is also shown.

B.1 Hockey-Puck Design with Added Inert Mass

In the BOOMERANG prototype described in Chapter 3, the magnet material comprises 83.1mg/92.7mg = 90% of the motional mass of the sensor oscillator. In practical microscopic designs, this ratio might vary substantially due to the realities of microfabrication, and so it is of interest to assess the effect of including inert mass (the silicon suspension) in the sensitivity optimizations for hockey-puck designs.

Figure 2.3 of Chapter 2 showed that for the case of no inert mass, the signal-to-noise ratio is not a sharply peaked function of either the sensor magnet's radius *a* or its height *h*. That figure is reproduced in Figure B.4 a with a larger range

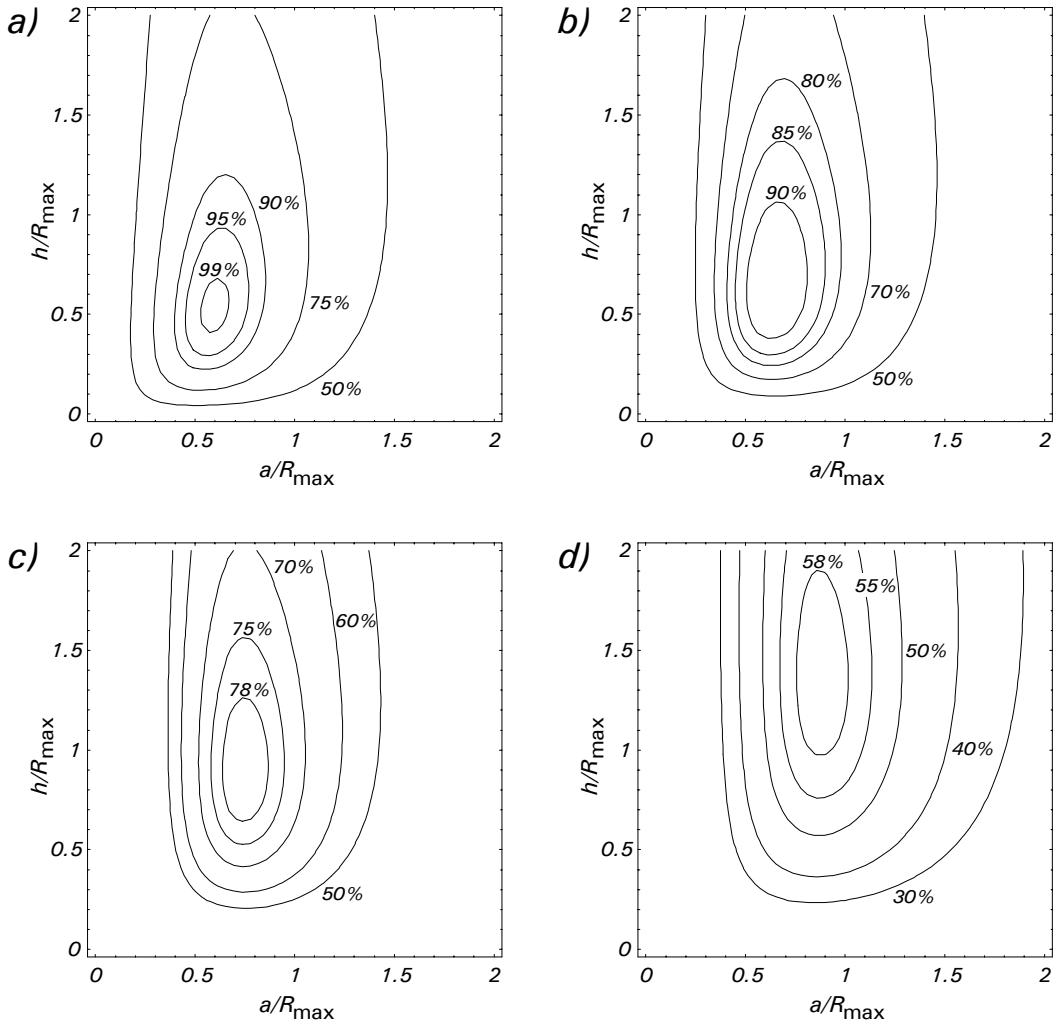

Figure B.4 Signal-to-noise ratio (*SNR*) vs. scaled radius a and height h of the sensor magnet. The contours show *SNR* relative to the *SNR* of the optimal design at $a/R_{max} = 0.59$ and $h/R_{max} = 0.53$ in Figure B.4 a, in which the suspension adds nothing to the oscillator's motional mass. a) No added inert mass. b) Inert mass 14.4% of Figure a's optimal mass, as in the BOOMERANG prototype. c) Inert mass equal to Figure a's optimal mass. d) Inert mass equal to five times Figure a's optimal mass.

of parameters. Figures B.4 b–d show contour plots of the SNR calculated for three other cases. In each case, the mass of the optimal sensor of Figure B.4 a is used as a fiducial mass. In Figure B.4 b, the effective mass of the silicon suspension is 14.4% of this fiducial mass. This is the relative mass of the silicon suspension used

in the BOOMERANG prototype. In Figure B.4 c, the case of an inert mass equal to the fiducial mass is shown, and in Figure B.4 d, the inert mass is five times the fiducial mass. The contours show that reasonably good *SNR* can be achieved over a wide range of design parameters when only mass and signal force are taken into account. A significant aspect of all of these graphs is that a $\sim$30% change in the radius *a* about its optimal value causes less than 5% loss in *SNR*, indicating that a small sacrifice in sensitivity could yield gains in homogeneity (with concomitant reduction in required rf power and heating of the oscillator and sample). More importantly, a more refined optimization procedure, which accounts for improved oscillator ring-down times associated with better sensor-annulus gap placement and spacing, should therefore have sufficient leeway to improve the sensitivity of next-generation BOOMERANG devices.

References

1 C. Lanczos, *The Variational Principles of Mechanics*, 4th ed. (Dover, New York, 1970), p. 59.

2 H. Goldstein, *Classical Mechanics*, 2nd ed. (Addison-Wesley, Reading, MA, 1980), p. 42.